

# Resonant nonlinear microscopy reveals changes in molecular level chirality in native biological tissues

M.-Y. Chen<sup>1</sup>, M. J. Huttunen<sup>2</sup>, C.-W. Kan<sup>1</sup>, G. Deka<sup>1</sup>, Y.-Y. Lin<sup>3,4</sup>, C.-W. Ye<sup>5</sup>, M.-J. Wu<sup>5</sup>, H.-L. Liu<sup>5</sup>, and S.-W. Chu<sup>1,6,\*</sup>

<sup>1</sup>Department of Physics, National Taiwan University, Taipei, Taiwan (R.O.C.)

<sup>2</sup>Department of Physics, University of Ottawa, 25 Templeton, ON, K1N 6N5, Canada

<sup>3</sup>Institute of Photonics Technologies, National TsingHua University, Hsinchu, Taiwan (R.O.C.)

<sup>4</sup>Department of Electrical Engineering, National TsingHua University, Hsinchu, Taiwan (R.O.C.)

<sup>5</sup>Department of Physics, National Taiwan Normal University, Taipei, Taiwan (R.O.C.)

<sup>6</sup>Molecular Imaging Center, National Taiwan University, Taipei, Taiwan (R.O.C.)

KEYWORDS: second-harmonic-generation; circular-dichroism; collagen; anisotropy

\* Correspondence should be addressed to Shi-Wei Chu. Email: [swchu@phys.ntu.edu.tw](mailto:swchu@phys.ntu.edu.tw).

Address: 1, Sec 4, Roosevelt Rd., Taipei 10617, Taiwan. Tel: +886-233665131; Fax: +886-223639984.

## ABSTRACT

Chirality is a fundamental property of biochemical molecules and often dictates their functionality. Conventionally, molecular chirality is studied by linear optical activity effects. However, poor contrast and artifacts due to anisotropy limit such studies to purified molecules not in their original microenvironments, potentially modifying their conformations. Here, we demonstrate that resonant second-harmonic-generation circular dichroism (SHG-CD) microscopy provides not only tissue imaging with improved chiral contrast, but also molecular chirality information of collagen, the most abundant protein in mammals, at its native state. Gradual protein denaturation shows that the resonant SHG-CD is dominated by the microscopic chirality related to collagen structures smaller than the spatial resolution of the microscope, i.e. to the protein conformation and microfibril organization, while the effects due to fiber orientation/anisotropy are mostly responsible of the non-resonant part. This result agrees well with a simple and intuitive model we propose to explain the resonant behavior and the consequent numerical SHG-CD simulations. Our results demonstrate the possibility to study molecular chirality in intact bio-tissues with nearly-unity contrast and sub-micrometer resolution, which will be useful in a broad range of biological and biochemical applications.

## 1. Introduction

Many molecules exist in left- or right-handed forms that are mirror images of each other, similar to human hands. This property is called chirality, and most biological molecules are chiral due to their complicated three-dimensional conformation. Even if the chemical compositions of the enantiomers are exactly the same, it is well known that the handedness of the molecules crucially affects the correct functioning of bio-molecules, including proteins, nucleic acids and sugars. Since molecular conformation and hence its chiral response is very sensitive to local chemical/physical conditions, it is vital to develop a tool that is able to investigate chiral molecules under their original microenvironments.

Conventionally, chiral materials are studied using linear optical-activity (OA) effects, such as optical rotatory dispersion and circular dichroism (CD) [1-3]. Interestingly, the CD response is enhanced near molecular resonances, providing the basis for utilizing CD spectroscopy as a powerful tool for studying secondary structures of proteins and to detect the denaturation of chiral polypeptides. The downside of CD spectroscopy is that the CD response requires light-matter interactions beyond the electric-dipole approximation, resulting in very weak relative signal strengths, i.e. contrast, on the order of 0.001. However, it is well known that anisotropy due to macroscopic molecular arrangement can also create artifacts in linear CD with signal strength on the order of 0.1 [4]. Therefore, CD studies are largely limited to purified molecules, and it is extremely difficult to study chiral molecules in complicated biological tissues based on linear OA responses.

In addition to linear OA effects, several nonlinear OA effects have been found, which can also provide information of the microscopic molecular structure [5]. Such effects include Raman OA [3], two photon absorption circular dichroism [6,7], chiral sum-frequency generation spectroscopy [8,9], and second-harmonic-generation circular dichroism (SHG-CD) [10-12]. Among them, some of the highest so far reported contrasts have been for SHG-CD, where the relevant chiral information could be accessed by measuring the normalized differences of second-harmonic generation (SHG) between right-handed circularly polarized (RCP) and left-handed circularly polarized (LCP) polarized fundamental laser beam [13]

$$SHG - CD = \frac{I_{RCP}(2\omega) - I_{LCP}(2\omega)}{[I_{RCP}(2\omega) + I_{LCP}(2\omega)]/2} . \quad (1)$$

SHG-CD was first discovered using purified chiral binaphthol molecules adsorbed on an air–water interface [10] and was later demonstrated in Langmuir–Blodgett films [14,15]. These studies showed that the SHG-CD can occur already within the electric-dipole approximation, explaining why its relative strength could be several orders of magnitude stronger than that of linear CD [10]. In addition, utilization of nonlinear processes like SHG-CD, provides extra advantages for imaging applications, such as intrinsic optical sectioning capabilities and improved penetration depth [16-18]. Combining these advantages, SHG-CD is a viable candidate for three-dimensional chiral imaging applications [19-24].

However, the origins of SHG-CD signals in intact biological tissues are not yet fully understood. Previous studies have shown that similar to linear OA effects, SHG-CD effects can also be influenced by sample anisotropy and orientation challenging its use to, for example study changes in protein secondary structures [25,26]. The issue of differentiating signals due to

sample anisotropy and the actual molecular chirality, related also to protein conformation, can be especially challenging for real bio-tissues, since such samples are in practice always anisotropic. A recent study demonstrated that in a sliced collagenous tissue, the contribution due to anisotropic orientation of collagen fibers dominates the SHG-CD responses with 1040-nm excitation [23]. Similar mechanism was found for SHG-CD of polysaccharides in starch granules [24]. To our knowledge, only two SHG-CD study so far has claimed to detect SHG-CD response of collagenous tissues [22,27], but the reported contrast was small, and it was not certain whether the signal originated dominantly from chirality or anisotropy.

An unambiguous tissue imaging modality capable to differentiate between the possible contributions due to microscopic molecular chirality, e.g. due to protein conformation, and due to sample anisotropy is a long-sought tool to study complicated chiral systems. Since SHG-CD responses are, analogous to linear CD, expected to be enhanced near molecular resonances [25,26,28,29], resonant SHG-CD imaging is anticipated to solve the existing ambiguity and provide chiral contrast in tissues.

In this work, we demonstrate that in an intact biological tissue, spectral SHG-CD microscopy can explicitly provide information of protein structures smaller than the spatial resolution when the fundamental excitation wavelength coincides with molecular resonances of the proteins. The protein target of investigation is type I collagen, which is the most abundant protein in the human body, and exhibits a special chiral structure composed of three polypeptide strands in a left-handed conformation that twist together to form a right-handed triple helix configuration [30]. Misfolding of the triple helices has been linked to various serious diseases [31-34]. Hence, it is important to be able to investigate the structural properties of type I collagen, especially under its

original microenvironment. We also propose a simple model predicting strongly wavelength-dependent SHG-CD responses near molecular resonances, and perform extensive numerical SHG-CD simulations, which show that the non-resonant SHG-CD responses are dominated by the sample anisotropy due to fiber orientation and crimping. However, the numerical results also show that the SHG-CD responses near molecular resonances can be dominated by the molecular chirality, related to collagen protein conformation and microfibril organization.

In order to verify these predictions, we perform spectral SHG-CD microscopy of collagenous samples by scanning the wavelength of the incident field from 750 – 1300 nm and show that the SHG-CD responses qualitatively change when the incident wavelength coincides with material resonances occurring near 900 nm. We further study the effects of fiber crimping and protein denaturation on the SHG-CD responses by performing simultaneous SHG-CD measurements while denaturing the protein samples via gradual heating. The collagen crimp pattern and fiber orientation is seen to dominate the off-resonant SHG-CD responses, while the resonant SHG-CD responses decrease in correlation with the protein denaturation. Therefore, our results show promise that spectral SHG-CD microscopy could be used as a viable technique to study structural changes in tissues.

## **2. Results**

### **2.1. SHG-CD microscopy in collagenous tissue**

Figures 1(a) and 1(b) show SHG images from type I collagen using excitation wavelength of 1040 nm for RCP and LCP excitations, respectively. A characteristic crimping pattern of the collagen fibers is observed. It is obvious that the outlines of these two images are the same, but

the actual intensity patterns are quite different. As defined by Eq. (1), SHG-CD can be calculated for each pixel from Figs. 1(a) and 1(b), resulting in the SHG-CD image shown in Fig. 1(c). As expected, the SHG-CD signal could reach unity, which is much larger than that of conventional linear CD. However, both positive and negative SHG-CD values are observed. This does not imply that both right- and left-handed molecular chirality simultaneously exist in the collagen, since based on our previous study [23], the positive and negative values of SHG-CD are mostly due to the collagen fiber orientation and crimping.

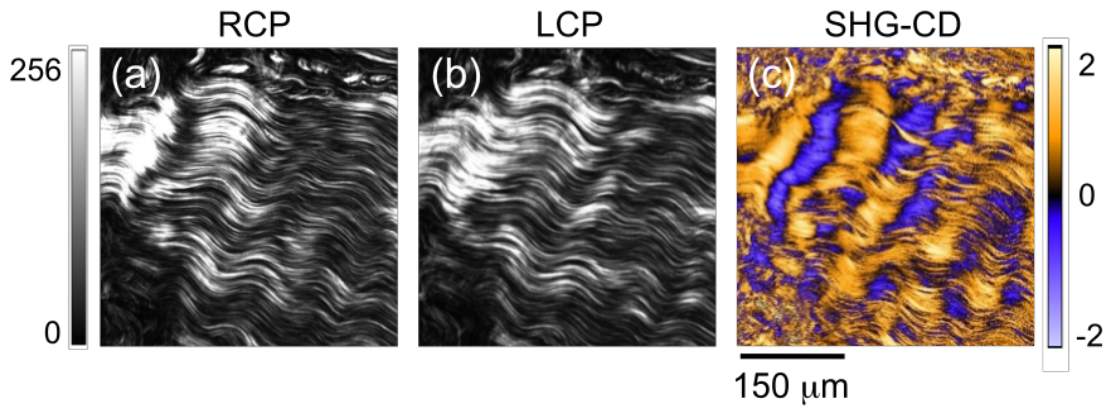


Fig. 1. (a) and (b) are SHG-intensity images using RCP and LCP input, respectively, at incident wavelength of 1040 nm. (c) Corresponding SHG-CD image obtained by using Eq. (1).

## 2.2 Spectral SHG-CD microscopic imaging

Figure 2 shows the optical absorption spectrum of type I collagen in the range of 500-2000 nm. The spectrum shows water absorption bands around 1400 nm and 1900 nm due to overtones of vibrational modes [35,36]. Specifically, the ~1400 nm peak corresponds to the summation of symmetric ( $3277\text{ cm}^{-1}$ ) and asymmetric ( $3490\text{ cm}^{-1}$ ) stretch, while the ~1900 nm peak is a mixture of the stretch and bend modes of water [37]. In addition, type I collagen exhibits an absorption band around 700-1000 nm [38], peaking near 835 nm. Because resonant behavior of

SHG-CD should be directly related to the molecular chiral structure, and to not sample anisotropy, we expected to see enhancement of SHG-CD response near this 835 nm resonance, while having a non-resonant background due to anisotropy effects from fiber orientations. This hypothesis was also backed up by a simple model we proposed here to elucidate the possible molecular origins of the resonant behavior of the SHG-CD responses (see Methods). We use the model to estimate the nonlinear molecular responses near a resonance and performed consequent numerical SHG-CD simulations on sample structures resembling collagen fibers using an approach based on Ref. [39], where the effects of molecular level chirality related to the protein conformation and microfibril organization, fiber orientation and collagen crimping pattern on the expected SHG-CD were studied, as will be discussed in a later section.

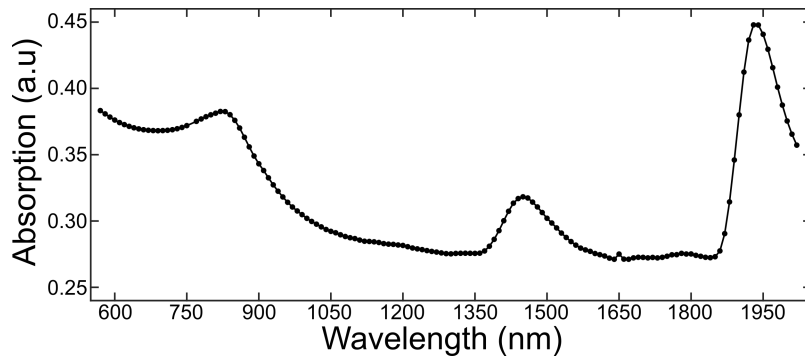


Fig. 2. Optical absorption spectrum of type I collagen tissue in the range of 500-2000 nm.

We measured a series of SHG-CD responses in the same focal plane with different excitation wavelengths (750-1300 nm, corresponding to SHG at 375-650 nm) using a Ti:sapphire oscillator and an optical parametric oscillator, as shown in Fig. 3(a-k). The SHG-CD image at 900-nm excitation appears clearly brighter from the rest. Fig. 3(l) shows the subtraction of the 900 nm and 950 nm SHG-CD images. The image color is almost completely orange, indicating that the SHG-CD values of most of the area increase when approaching resonance, but we note that this

increase does not directly imply an increase in the overall SHG. This pixel-by-pixel analysis shows that although the varying SHG-CD at non-resonant excitation seems to be mostly due to fiber orientation and crimping [see for example Fig. 3(i)], the SHG-CD at resonant excitation near 900 nm becomes mostly positive. We repeated these SHG-CD imaging measurements (at room temperature) for four different samples. The resulting SHG-CD spectra, averaged from all four samples, are shown in Fig. 3(m), where despite statistical variations, a peak near 900 nm is visible, roughly coinciding with the linear absorption peak of collagen in Fig. 2. The red-shift of the SHG-CD peak versus the linear absorption peak will be discussed later.

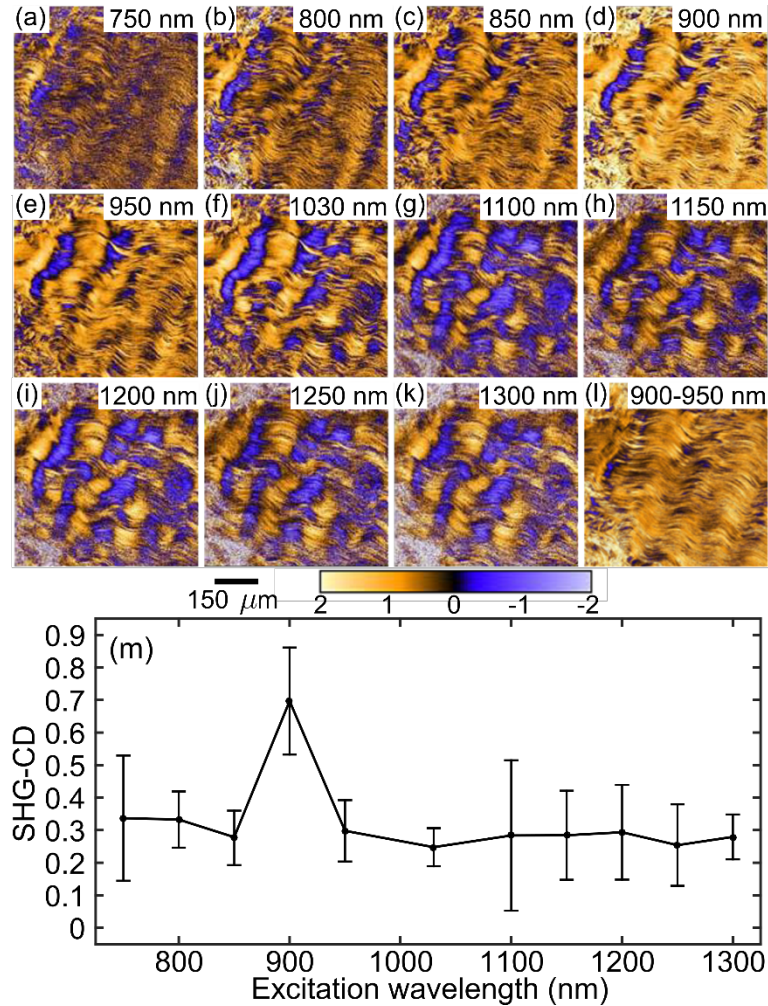


Fig. 3 (a-k) SHG-CD images for different excitation wavelengths in the range of 750-1300 nm. Positive, zero, and negative SHG-CD values are shown as orange, black, and blue, respectively. (l) The difference between the 900 and

the 950 nm images show that the SHG-CD values are higher at resonance. (m) Averaged SHG-CD spectra of type I collagen tissues.

The SHG-CD values are fairly stable at  $\sim 0.3$  for non-resonant excitation wavelengths (750-800 nm, 1000-1300 nm), as is seen in Fig. 3(m). We attribute this SHG-CD background to the average contribution from the anisotropy and orientation of collagen fibers. The value of this SHG-CD background corresponds well to the results of our previous work, where a 1040 nm femtosecond laser was used [23].

### **2.3 Effect of protein denaturation on the SHG-CD response**

In order to further confirm our result, we acquire SHG-CD spectra while gradually denaturing the proteins by heating the sample. Since the collagen molecules dissociate at temperature range of 53-57°C, their molecular chirality should disappear above this temperature range [40,41]. On the other hand, we have recently found that before denaturation, at lower temperature heating, the crimp pattern of collagen fibers vanishes [42]. Therefore, if the non-resonant SHG-CD is mostly due to fiber orientation and crimping, it should vanish already at the lower temperatures. Nevertheless, the molecular triple-helix structure and the microfibril organization of the collagen proteins is unaffected at this low temperature range, and therefore molecular contribution to the SHG-CD should persist until temperatures over 53°C are reached.

With the above knowledge, we heated the collagen samples in steps from 25°C to 70°C, and the corresponding SHG-CD spectrum degradations are shown in Fig. 4(a). Close inspection of Fig. 4(a) shows that the SHG-CD decreases in two stages, corresponding to different structural phase variations. In the first stage of heating, from 25°C to 40°C, the non-resonant SHG-CD

background of approximately 0.3 disappears due to the loss of collagen crimping. However, after this low-temperature heating process, the SHG-CD peak ( $\sim 0.4$ ) near 900 nm remains, suggesting its origin is due to molecular chirality.

The relationship between the resonant peak and the molecular chirality becomes more evident in the second stage of heating. From 40°C to 50°C, the pattern of the entire spectrum remains nearly constant, indicating no significant structural change of collagen at this temperature range. Then, in the range of 50°C to 60°C, the triple helix starts to denature, leading to loss of molecular chirality and significant decay of the SHG-CD resonant peak, while the SHG-CD values in the non-resonant regions remain approximately zero. Above 60°C, further decay of the resonant peak is observed, reflecting the ongoing loss of the molecular conformation and thus chirality. The two-stage heating process corresponds well to literatures [42,43].

In addition to experimental demonstrations, we also propose a model to explain the resonant SHG-CD responses and carried out consequent simulations to study the relationship between SHG-CD and protein denaturation process, as shown in Fig. 4(b). The numerical approach follows closely our recent work [39], and is explained along with the proposed model in more detail in Methods. First we simulated spectral SHG-CD responses from an individual crimped collagen fiber for the used excitation wavelength range. A resonant peak due to molecular level chirality along with a non-resonant background due to anisotropy and crimping of collagen fibers is seen in the black curve of Fig. 4(b). Then the crimp amplitude  $A$  was gradually reduced from 80 to 0 nm, reproducing the overall SHG-CD reduction in the first stage of the heating experiment. When the crimp amplitude  $A$  vanishes ( $A = 0$  nm), a resonant SHG-CD peak at 900 nm persists, manifesting its molecular level chirality origin. Finally, we studied the effect of

protein denaturation on the SHG-CD by decreasing the strength of the susceptibility components related to molecular level chirality. As expected, when the chiral component disappears ( $xyz = 0$ ), SHG-CD responses in practice vanish. In overall, the simulation results agree very well with the experiments, providing a solid foundation of our interpretation.

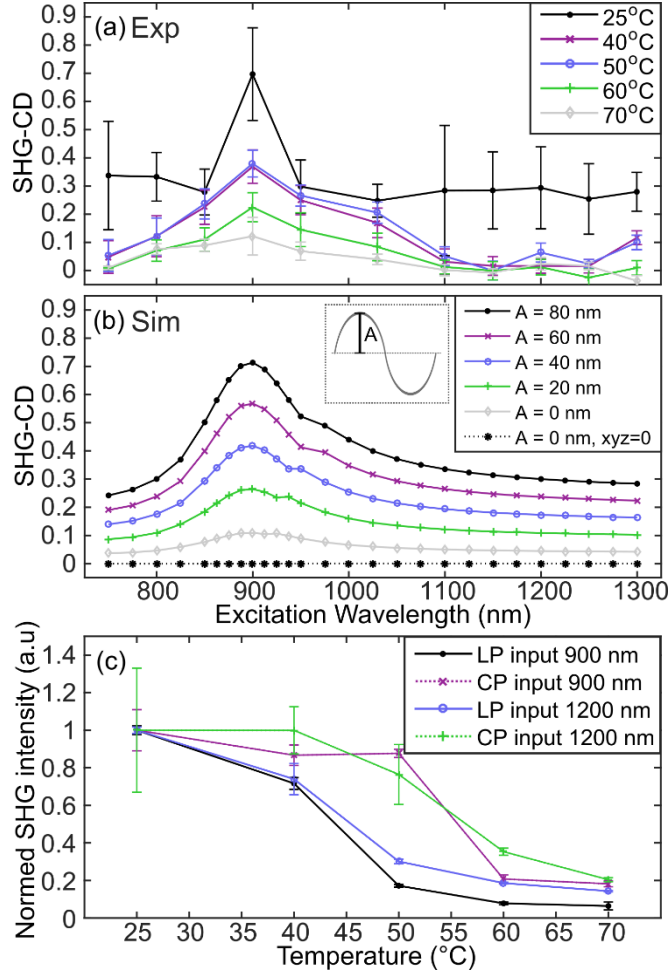


Fig. 4. (a) Averaged SHG-CD spectra of type I collagen under gradual protein denaturation. First, the gradual heating removes the crimp pattern of collagen leading to decrease in the overall SHG-CD. The peak for the excitation wavelength around 900 nm remains relatively unchanged, until the sample is heated over 53°C, after which the secondary helical structure of collagen starts to denature. (b) Simulated SHG-CD responses while gradually reducing the collagen crimping amplitude  $A$  from 80 nm to 0 nm. (c) The overall SHG intensities also change when the sample is heated. Results are shown for fundamental wavelengths at 900 and 1200 nm and using linearly polarized (LP) and circularly polarized (CP) excitations. When the sample was heated to 50°C, the overall SHG efficiency for LP input beam dropped to 25% of the initial value while the overall SHG efficiency for CP input was still at 90%.

In addition to the SHG-CD measurements, it is well known that the SHG intensity of linearly polarized excitation is more sensitive to the anisotropic orientation of collagen fibril than circularly polarized excitation [44]. Therefore, to further verify the existence of the anisotropy loss at the first stage of heating, the overall SHG intensities obtained with linearly polarized and circularly polarized excitations were measured as a function of temperature, as shown in Fig. 4(c). If the change during heating from 25°C to 50°C is primarily related to fiber anisotropy, SHG with linear polarization should drop faster than SHG with circular polarization. This is exactly what we observed in Fig. 4(c). Interestingly, irrespective of whether the excitation wavelength is resonant (900 nm) or non-resonant (1200 nm), a similar tendency is observed for linear and circular polarizations, indicating that the anisotropy of the collagen fibers changes substantially during the low-temperature heating, and that the anisotropy effect is wavelength-independent.

For more quantitative understanding, the variation of RCP SHG and LCP SHG at 900 nm and 1200 nm are listed in table 1. At low temperature (25-50 °C), it is mainly the reduction of RCP SHG that causes the reduction of CD when temperature increases. At high temperature (60-70 °C), both RCP and LCP SHG show significant reduction, resulting in further decrease of CD value. Comparing the data of resonant 900nm and non-resonant 1200nm, the reason that SHG-CD is increased at resonance is because of both larger RCP and lower LCP values.

Table 1. The relative SHG intensity with RCP and LCP excitations derived from Fig. 4, at resonant (900 nm) and non-resonant (1200 nm) fundamental wavelengths. The values are normalized to the RCP+LCP value at room temperature for each wavelength.

Temp (°C)	RCP+LCP (Fig. 4c)	SHG-CD = 2(RCP-LCP)/(RCP+LCP) (Fig. 4a)	RCP - LCP	RCP	LCP
900 nm					
25	1.00	0.70	0.35	1.35	0.65
40	0.87	0.37	0.16	1.03	0.71
50	0.88	0.38	0.17	1.04	0.71
60	0.21	0.22	0.02	0.23	0.18
70	0.18	0.12	0.01	0.19	0.17
1200 nm					
25	1.00	0.29	0.15	1.15	0.85
40	1.00	0.02	0.01	1.01	0.99
50	0.76	0.06	0.02	0.79	0.74
60	0.35	0.01	0.00	0.36	0.35
70	0.20	0.02	0.00	0.21	0.20

### 3. Discussion

In this work, we first measure absorption spectrum of collagen tissues, and then acquire SHG-CD microspectroscopic images from the same type of tissue. From Fig. 3, it is obvious that the SHG-CD signal at resonance near 900 nm [see Fig. 3(d)] behaves qualitatively different from the non-resonant SHG-CD (see the other panels of Fig. 3). The results serve as a hint that the SHG-CD contributions from molecular level chirality and from anisotropy due to fiber orientations can be differentiated by spectral measurements. This prediction is further supported by the protein

denaturation study in Fig. 4, where the anisotropy contributed SHG-CD disappears at lower temperatures (25°C to 50°C), while the microscopic chirality related contribution remains until higher temperatures above 50°C are reached. To our knowledge, our result is the first to unambiguously distinguish these different contributions to SHG-CD, under the complex microenvironment of intact biological tissues, demonstrating the direct applicability of our results.

First, we discuss birefringence as a possible source of artifacts in the measured SHG-CD responses. In general, tissues are anisotropic and thus birefringent. Therefore, propagation of the fundamental beam inside the tissue sample does alter its polarization state [45]. Since the SHG-CD measurements depend sensitively on the polarization of the fundamental beam, effect of this linear birefringence should be accounted for. Additional experiments were carried out to quantify the birefringence of the collagenous tissue (anterior cruciate ligaments) in our experiment, and the resulting  $\Delta n$  is 0.004, agreeing well to recent literature [46,47]. Therefore, when the imaging depth is at 10  $\mu\text{m}$ , the retardation is 40 nm, corresponding only to  $\lambda/20$  delay for an 800-nm excitation wavelength. Such a retardation causes still negligible artifacts for SHG-CD measurements, and is less critical for longer wavelength experiments. However, if imaging is performed from deeper than 20  $\mu\text{m}$ , the accumulated phase delay can be larger than  $\lambda/10$ , and great care must be taken to interpret the SHG-CD (and all other polarization dependent SHG) results [45].

A relevant note is that since the SHG-CD values in Fig. 3m are averaged from four samples, if all the fibrils are randomly oriented, the SHG-CD average is expected to vanish. However, since

we prepared the samples with the same procedure from similar regions of tendons, the fibril orientations are not random, resulting in the residual SHG-CD value from the macroscopic structural chirality.

On the other hand, we also would like to point out that the main result in this work is based on microspectroscopy, which shows that the SHG-CD image contrast at 900-nm is different from neighboring wavelengths, such as 850-nm, while the birefringence of collagen tissues at 900-nm is similar to that at 850-nm. That is, although the absolute magnitude of SHG-CD signal may still be affected by sample birefringence due to changes in the circular polarization of the fundamental beam, the birefringence and consequent polarization scrambling cannot explain the spectral behavior of the measured SHG-CD response.

We discuss next the possible origins of the measured SHG-CD peak when the fundamental excitation is near 900 nm. First we note, that collagen type I exhibits a broad fluorescence emission peak at 400-500 nm, but the origin of this peak is not well understood [48]. Since the quantum mechanical expression for the second-order susceptibility depends on the optical properties of the material both at the fundamental and at the second-harmonic wavelength [49], the resonances related to the broad fluorescence peak could play a role in the measured SHG-CD peak.

According to a simple but intuitive resonant SHG-CD model we propose here (see Methods), molecular resonances at the fundamental wavelength can give rise to wavelength-dependent SHG-CD responses, if the resonant chromophores are organized in a chiral configuration, such as in a helix. In the proposed model, we assume that the measured absorption peak near 835 nm

(see Fig. 2) is due to chemical bonds, organized into a helical configuration, and that the nonlinear molecular response follows their linear resonant behavior [12]. The calculated macroscopic nonlinear response and the consequent SHG-CD responses then show resonant behavior near 900 nm (see Figs. 4a and 4b). The red-shift of the SHG-CD peak with respect to the absorption peak near 835 nm was attributed to the complex interference effects in the detected SHG emission, where the phase distribution of the excitation field and all the non-zero susceptibility components together are responsible of the measured SHG-CD response. Therefore, it is interesting to try to understand the possible origins of the measured absorption peak near 835 nm. According to literature, the fourth overtone of C-H stretching mode in alkane group of collagen is located near 900 nm [50], which we believe is also visible in the measured absorption spectrum (see Fig. 2). Interestingly, the overtone modes of the C-H stretch have been earlier attributed with chiroptical responses [51]. Therefore, we suspect that they play a dominant role in the measured SHG-CD responses.

We conclude the discussion on the possible origins of the SHG-CD peak by admitting that the exact origin is not yet fully understood. But since the proposed SHG-CD model agrees very well with the measured SHG-CD spectra, we suspect that the chemical bonds responsible of the measured absorption peak near 835 nm play a dominant role in the SHG-CD response. In particular we think that the C-H stretch and its overtone or combination modes play a major role due to their verified optical activity near 900 nm [51]. It is interesting to note that in linear CD studies with a large molecular system [52], spectral red-shift between absorption peak and peak of CD response is also observed, but the underlying mechanism is not well explained yet.

As we have mentioned earlier, collagen molecules form an interesting helical structure, i.e. left-handed chirality in the polypeptide chain, and right-handed chirality in the triple helix structure. From Fig. 4, after the loss of collagen crimping by heating to 40°C, we observed positive SHG-CD; that is, SHG using RCP input polarization is stronger than with LCP input. However, this does not imply that SHG-CD visualizes the chirality of the triple helix. In our current work, second-order nonlinear susceptibilities are used to simulate SHG-CD response in Fig. 4(b). To unravel the link between the nonlinear susceptibilities and molecular conformation, more detailed spectral analysis along with *ab initio* simulation will be required. But, since the resonant SHG-CD is seen to be related to molecular level chirality, i.e. to protein conformation and microfibril organization, changes in SHG-CD values could in principle be used to provide information of conformational changes. This is an interesting possibility, since our setup is relatively simple compared to other possible approaches based on sum-frequency generation spectroscopy and oblique angles of incidence [8,9,12,53,54]. Most importantly, we use a single excitation beam and perform laser-scanning microscopy providing information with a spatial resolution close to 600 nm.

As a final remark, we showed in Fig. 4 that non-resonant SHG-CD is related to the crimp pattern of collagen. Though the main theme of this work is to study molecular level chirality, such macroscopic information could actually be useful when studying collagenous tissue mechanics [55] as well as wound healing process [56]. In addition, SHG imaging has been demonstrated for *in vivo* microscopy or endoscopy applications [57]. By playing with resonant and non-resonant SHG-CD, noninvasive detection of both molecular and macroscopic structural properties of collagenous tissues will open up entirely new possibilities.

## **4. Conclusion**

In conclusion, we performed SHG chiral microspectroscopy for type I collagen tissue with excitation wavelengths in the range of 750–1300 nm. We verified that two main mechanisms exist for SHG-CD in an intact biological tissue: fiber anisotropy and orientation and molecular level chirality due to protein conformation and microfibril organization. Most importantly, we show that molecular level chirality can be probed using SHG-CD only at resonant wavelengths. For non-resonant wavelengths, SHG-CD contrast provides dominantly information on the fiber orientations and anisotropy. We demonstrated that the molecular (resonant) and anisotropy-related (non-resonant) contributions could be differentiated via temperature- and polarization-dependent measurements. To our knowledge, this is the first successful demonstration to probe molecular level chirality of proteins under their original bio-tissue microenvironment. Our investigation paves the way toward a realistic SHG-CD microspectroscopic tool for studying chirality in three-dimensional biological samples. Since the molecular level chirality is also related to molecular conformation, spectral SHG-CD microscopy could possibly be used to study conformational changes, which for example in tissues are related to several severe diseases.

## **5. Methods**

### **5.1 Spectral SHG-CD microscopy**

Our experimental setup is shown in Fig. 5. A tunable Ti:sapphire femtosecond laser (Chameleon-Vision II, Coherent, USA) and an optical parametric oscillator (OPO) provided excitation wavelengths in the range of 750–1300 nm. A set of polarizing beam splitters (PBSs) and half-wave plates (HWPs) were used to maintain the power at 30 mW in the back aperture of

the objective lens under various wavelengths. This power level was chosen to ensure a good signal-to-noise ratio and that no sample degradation for example via heating occurs, which was verified by measuring signals with good repeatability over the entire excitation wavelength range. The excitation light was directed into a Leica TCS SP5 system with a pair of X-Y galvanometers to achieve raster scanning, and the light was focused onto the specimen using an objective lens (HC PL IRAPO 20X, NA=0.75 water immersion, Leica). This specially designed objective lens has high transmission from visible to 1300-nm wavelength region and provides exceptional axial and lateral color-aberration correction throughout its spectral transmission range.

The SHG signals were collected by a condenser in the forward direction and detected with a photomultiplier tube (PMT). A short-pass filter that blocks wavelengths above 890 nm (FF01-890/SP-25, Semrock, USA) for 1100–1300 nm excitation and one that blocks wavelengths above 550 nm (SPF-550-0.50, CVI Laser Optics, USA) for 750–1050 nm excitation were placed, respectively, in front of the PMT to ensure the effective suppression of excitation. Since two-photon fluorescence of collagen is diminishing, especially when excited with wavelength longer than 800 nm [58], no narrow-band-pass filter is placed in the detection path. A Soleil–Babinet compensator (SBC-IR, Thorlabs, USA) was placed in front of the scanner to achieve high-quality circularly polarized light. For each wavelength, an optimal configuration of the SBC was determined to ensure that the ellipticity of circular polarization was less than 1.05 at the focus. Circularly polarized light of opposite handedness could be generated by rotating the half-wave plate in front of the SBC. This experimental setup allows the study of the wavelength dependence of SHG-CD signals.

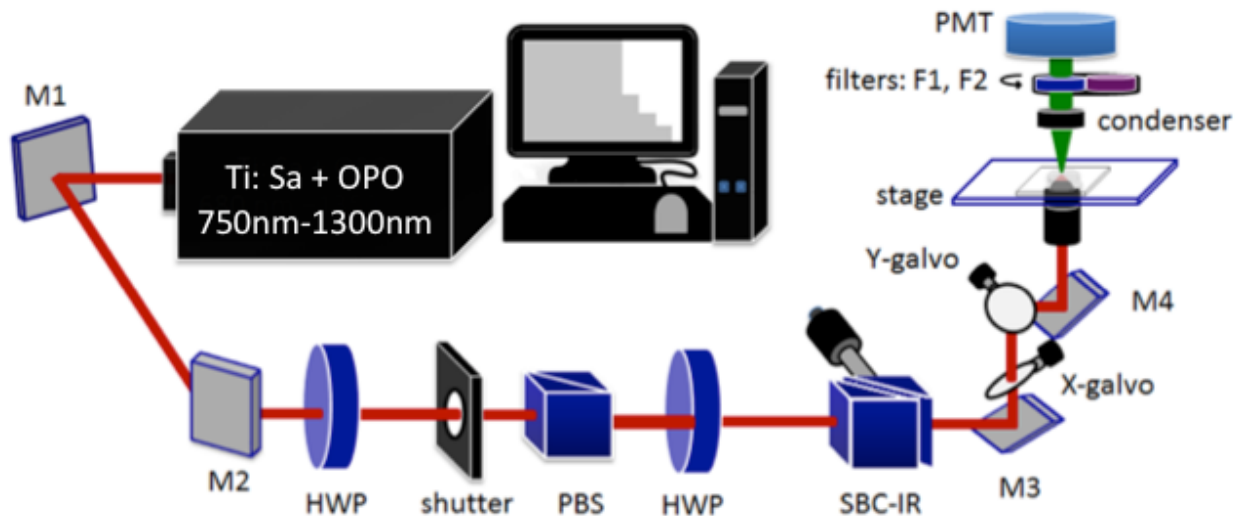


Fig. 5. Setup of a spectroscopic SHG-CD microscope. M1-M4: mirrors; HWP: half-wave plate; PBS: polarization beam splitter; SBC-IR: Soleil-Babinet compensator for infrared; F1: short-pass filter with a 550 nm cutoff; F2: short-pass filter with an 890-nm cutoff; PMT: photomultiplier tube.

## 5.2 Sample preparation

The type-I collagen sample was harvested from anterior cruciate ligaments of freshly slaughtered porcine knee joints, which were commercially purchased. We used a Leica CM1950 clinical cryostat to prepare 20- $\mu$ m-thick tendon sections. The specimens were immersed in isotonic sodium-chloride solutions (each ml contained 9.0 mg of sodium chloride) and were each placed between a coverslip and a glass slide. The edges of the coverslips were sealed to minimize the effects of hydration on the collagen denaturation. The optical absorption of type I collagen was studied using a UV/VIS/NIR spectrometer (Lambda 900, PerkinElmer, USA). In the collagen denaturation measurement, the slides were placed on a custom-made graphite heater, and each slide was maintained at a certain temperature for 15 min (40°C, 50°C, 60°C, and 70°C).

Please note that compare to [42], the heating process is much slower here, so it may result in different threshold values in the thermal response.

### 5.3 SHG-CD simulations

Simulations to understand how molecular resonances and the denaturation process can affect the SHG-CD responses were performed using an approach based on Green's functions and Rayleigh-Gans approximation [39]. In short, the circularly polarized incident field was assumed to be focused into the sample volume by an objective identical to the experimental setup (NA=0.75). The tight focusing condition results in a field distribution, which has a non-negligible longitudinal field component, i.e. a field component oscillating along the optical axis. The longitudinal component was calculated to be on the order of 5 % of the total field strength, and therefore we decided to use an approach based on full vector diffraction theory [39]. We further studied the effect of the longitudinal field on the simulated SHG-CD responses, and found out that if the longitudinal field component was neglected, the simulated SHG-CD responses decreased ~25 % near the molecular resonance and ~60 % at off-resonant conditions. We note that the non-zero SHG-CD responses in these simulations (zero longitudinal field component) were due to the high NA collection scheme. In plane wave approximation, i.e. when both the incident and the detected fields are approximated as plane waves propagating normal to the sample plane, the simulated SHG-CD responses vanish. Therefore, we conclude that performing the simulations while using the full vector diffraction theory, and by fully taking into account the high NA of the collection objective, was the appropriate choice.

The focused vector field interacted with the nonlinear medium and gave rise to a nonlinear source polarization, being responsible of the second-harmonic emission. We assumed, that electric dipole approximation holds and negligible coupling occurs between the second-harmonic harmonophores. Then the emission and propagation of the second-harmonic signal through the condenser and into the detector can be calculated using free-space Green's function approach [39]. The SHG-CD values were then calculated by changing the handedness of the circularly polarized incident field and simulating the corresponding second-harmonic emission.

Performing ab initio calculations to model resonant second-order responses of collagen molecules is beyond the current computational capabilities. Therefore, simpler models to qualitatively understand the origins of the resonant SHG-CD response have to be used. Here, we used a model where the collagen susceptibility was calculated as a sum of molecular harmonophores, ordered into a triple-helix resembling the structure of tropocollagen [23,39,41]. We neglected possible coupling between the harmonophores, after which the non-zero chiral susceptibility components were solely due to the helical organization of the harmonophores [11,59]. For simplicity, we assumed that the harmonophores were identical and belonged to a symmetry group of  $C_{\infty v}$ . The non-zero hyperpolarizability components of each harmonophore are then  $zzz$ ,  $zxx=zyy$  and  $xxz=xzx=yyz=yyz$ , in the molecular coordinate system where  $z$  points along the long axis of the harmonophore. We further simplified the model by assuming that the nonlinear response of the harmonophores is restricted to  $xz$ -plane, resulting in three non-zero components of  $zzz$ ,  $zxx$ , and  $xxz=xzx$ . This assumption is appropriate if the molecular response is mostly due to chemical bonds and their activity restricted into a single plane. When such harmonophores were arranged into a triple-helix resembling tropocollagen (Proper Euler angles,

$\theta=52^\circ$ ,  $\psi=20^\circ$  and varying  $\phi$  formed the helical spiral), the resulting susceptibility belonged to a chiral symmetry group of  $C_\infty$  allowing thus in principle non-zero SHG-CD responses [23].

The resulting SHG-CD responses did not yet show wavelength-dependent behavior, which could be incorporated into the model by assuming that some of the hyperpolarizability components showed resonant behavior. We measured an absorption peak near 835 nm (see Fig. 2). According to the quantum mechanical expression for the nonlinear molecular response, the hyperpolarizability depends on the linear response of the molecule both at the fundamental wavelength and at the second-harmonic wavelength [49]. Based on this, we assumed that the molecular hyperpolarizability components  $xxz=xzx$  were affected by the resonance near 835 nm while the  $zzz$  and  $zxx$  components remained non-resonant and had relative values of 0.4 and 0.2, respectively. The maximum relative amplitude of the resonant  $xxz=xzx$  components was 0.33 at the 835 nm. We further assumed that the resonance followed a Lorentzian lineshape and found the corresponding lineshape parameters by fitting a Lorentzian line profile to the measured absorption spectrum. The fitted peak wavelength was 835 nm and the lifetime of the resonance was 1 fs. The resulting susceptibility tensor then became complex-valued where the different tensor components also had different relative phases. We list the resulting relative nonzero susceptibility tensor components at resonant (non-resonant) wavelength of 900 nm (1200 nm) in Table 2, where it is seen that even relatively small changes in the susceptibilities can result in different SHG-CD responses. According to the theory regarding nonlinear optical activity effects, non-zero SHG-CD occurs when a phase difference between chiral and achiral susceptibility components exist [26]. Therefore, this simple proposed model already qualitatively predicts wavelength-dependent SHG-CD responses and provides an intuitive basis for understanding the

origins of the SHG-CD response (see the imaginary parts in Table 2). Interestingly, the proposed model also correctly predicted the measured red-shift between the absorption peak (at 835 nm) and the SHG-CD peak (near 900 nm). Therefore, we believe that the proposed simple model already adequately describes the occurring physics and provides a good starting point to understand the wavelength-dependent SHG-CD responses. But we also admit that further experimental and theoretical work is probably needed to develop a more quantitative model.

Table 2. Calculated relative nonzero susceptibility components at resonant (900 nm) and non-resonant (1200 nm) fundamental excitation. The values are normalized with respect to each  $zzz$ .

Nonzero susceptibility component	$zzz$	$zxx$	$xyx$	$xyy$
Fundamental beam at 900 nm	0.61-0.13i	1	0.18-0.30i	0.26-0.10i
Fundamental beam at 1200 nm	0.70-0.01i	1	0.39-0.03i	0.20-0.01i

During protein denaturation, first the collagen protein crimping pattern vanished after which the protein conformation started to degrade. In the simulations, the crimp pattern was approximated by bending the simulated collagen fiber into a sinusoid with a maximum amplitude of 80 nm, which is less than the observed maximum crimp amplitudes in the used samples (see for example Figs. 1 and 3). The spectral SHG-CD responses during the first denaturation step were then simulated by gradually decreasing the crimp amplitude from 80 nm to 0 nm in steps of 20 nm. The SHG-CD responses after the final denaturation stage were simulated by decreasing the chiral susceptibility components to zero. The simulation results are shown in Fig. 4(b) and agree very well with the performed denaturation experiments.

## Acknowledgements

This study was supported by the Ministry of Science and Technology, Taiwan, under grant MOST-106-2321-B-002-020- and MOST-105-2628-M-002-010-MY4. SWC acknowledge the generous support from the Foundation for the Advancement of Outstanding Scholarship. MJH acknowledges the support from Finnish Cultural Foundation (00150020).

## REFERENCES

- [1] E. Charney, *The molecular basis of optical activity* (Wiley, NY, 1979).
- [2] P. J. Stephens, F. J. Devlin, C. F. Chabalowski, and M. J. Frisch, *J. Phys. Chem.* **98**, 11623 (1994).
- [3] L. D. Barron, *Molecular Light Scattering and Optical Activity* (Cambridge University Press, 2009).
- [4] J. H. Freudenthal, E. Hollis, and B. Kahr, *Chirality* **21**, E20 (2009).
- [5] P. Fischer and F. Hache, *Chirality* **17**, 421 (2005).
- [6] I. Tinoco, *J. Chem. Phys.* **62**, 1006 (1975).
- [7] C. Toro, L. De Boni, N. Lin, F. Santoro, A. Rizzo, and F. E. Hernandez, *Chem. Eur. J.* **16**, 3504 (2010).
- [8] E. C. Y. Yan, L. Fu, Z. G. Wang, and W. Liu, *Chem. Rev.* **114**, 8471 (2014).
- [9] J. Wang, X. Y. Chen, M. L. Clarke, and Z. Chen, *Proc. Natl. Acad. Sci. U. S. A.* **102**, 4978 (2005).
- [10] T. Petralli-Mallow, T. M. Wong, J. D. Byers, H. I. Yee, and J. M. Hicks, *J. Phys. Chem.* **97**, 1383 (1993).
- [11] G. J. Simpson, *Chemphyschem* **5**, 1301 (2004).
- [12] L. M. Hupert and G. J. Simpson, *Ann. Rev. Phys. Chem.* **60**, 345 (2009).
- [13] S. Sioncke, T. Verbiest, and A. Persoons, *Mater. Sci. Eng. R-Rep.* **42**, 115 (2003).
- [14] M. J. Crawford, S. Haslam, J. M. Probert, Y. A. Gruzdkov, and J. G. Frey, *Chem. Phys. Lett.* **230**, 260 (1994).
- [15] J. D. Byers, H. I. Yee, and J. M. Hicks, *J. Chem. Phys.* **101**, 6233 (1994).
- [16] P. J. Campagnola and L. M. Loew, *Nat. Biotech.* **21**, 1356 (2003).
- [17] S.-W. Chu, S.-Y. Chen, T.-H. Tsai, T.-M. Liu, C.-Y. Lin, H.-J. Tsai, and C.-K. Sun, *Opt. Express* **11**, 3093 (2003).
- [18] W. R. Zipfel, R. M. Williams, and W. W. Webb, *Nat Biotech* **21**, 1369 (2003).
- [19] M. A. Kriech and J. C. Conboy, *J. Am. Chem. Soc.* **127**, 2834 (2005).
- [20] R. M. Williams, W. R. Zipfel, and W. W. Webb, *Biophys. J.* **88**, 1377 (2005).
- [21] D. J. Kissick, D. Wanapun, and G. J. Simpson, *Annu. Rev. Anal. Chem.* **4**, 419 (2011).
- [22] X. Y. Chen, C. Raggio, and P. J. Campagnola, *Opt. Lett.* **37**, 3837 (2012).
- [23] H. Lee, M. J. Huttunen, K. J. Hsu, M. Partanen, G. Y. Zhuo, M. Kauranen, and S. W. Chu, *Biomed. Opt. Express* **4**, 909 (2013).
- [24] G. Y. Zhuo, H. Lee, K. J. Hsu, M. J. Huttunen, M. Kauranen, Y. Y. Lin, and S. W. Chu, *J.*

- Microsc. **253**, 183 (2014).
- [25] J. M. Hicks, T. Petrallimallow, and J. D. Byers, *Faraday Discuss.* **99**, 341 (1994).
  - [26] T. Verbiest, M. Kauranen, Y. VanRompaey, and A. Persoons, *Phys. Rev. Lett.* **77**, 1456 (1996).
  - [27] F. J. Avila, O. del Barco, and J. M. Bueno, *J. Opt.* **19**, 105301 (2017).
  - [28] H. Mesnil, M. C. Schanne-Klein, F. Hache, M. Alexandre, G. Lemerrier, and C. Andraud, *Phys. Rev. A* **66**, 013802 (2002).
  - [29] D. Catone, M. Stener, P. Decleva, G. Contini, N. Zema, T. Prosperi, V. Feyer, K. C. Prince, and S. Turchini, *Phys. Rev. Lett.* **108**, 083001 (2012).
  - [30] M. D. Shoulders and R. T. Raines, *Annu. Rev. Biochem.* **78**, 929 (2009).
  - [31] A. Vogel, K. A. Holbrook, B. Steinmann, R. Gitzelmann, and P. H. Byers, *Lab Invest* **40**, 201 (1979).
  - [32] B. Sykes, P. Wordsworth, D. Ogilvie, J. Anderson, and N. Jones, *The Lancet* **328**, 69 (1986).
  - [33] D. F. Holmes, R. B. Watson, B. Steinmann, and K. E. Kadler, *Chem. Phys. Lett.* **268**, 15758 (1993).
  - [34] M. C. Willing, S. P. Deschenes, D. A. Scott, P. H. Byers, R. L. Slayton, S. H. Pitts, H. Arikat, and E. J. Roberts, *Am. J. Hum. Genet.* **55**, 638 (1994).
  - [35] A. R. Duke, E. Peterson, M. A. Mackanos, J. Atkinson, D. Tyler, and E. D. Jansen, *J. Neural Eng.* **9**, 066006 (2012).
  - [36] G. M. Hale and M. R. Querry, *Appl. Opt.* **12**, 555 (1973).
  - [37] G. E. Walrafen and E. Pugh, *J. Solution Chem.* **33**, 81 (2004).
  - [38] P. Taroni, A. Bassi, D. Comelli, A. Farina, R. Cubeddu, and A. Pifferi, *J. Biomed. Opt.* **14**, 054030 (2009).
  - [39] M. J. Huttunen, M. Partanen, G. Bautista, S.-W. Chu, and M. Kauranen, *Opt. Mater. Express* **5**, 11 (2015).
  - [40] N. T. Wright and J. D. Humphrey, *Annu. Rev. Biomed. Eng.* **4**, 109 (2002).
  - [41] A. Deniset-Besseau, J. Duboisset, E. Benichou, F. Hache, P. F. Brevet, and M. C. Schanne-Klein, *J. Phys. Chem. B* **113**, 13437 (2009).
  - [42] C. S. Liao, Z. Y. Zhuo, J. Y. Yu, Y. Y. Tzeng, S. W. Chu, S. F. Yu, and P. H. G. Chao, *Appl. Phys. Lett.* **98**, 153703 (2011).
  - [43] P. Matteini, R. Cicchi, F. Ratto, D. Kapsokalyvas, F. Rossi, M. de Angelis, F. S. Pavone, and R. Pini, *Biophys. J.* **103**, 1179 (2012).
  - [44] X. Chen, O. Nadiarynykh, S. Plotnikov, and P. J. Campagnola, *Nat. Protocols* **7**, 654 (2012).
  - [45] D. Ait-Belkacem, A. Gasecka, F. Munhoz, S. Brustlein, and S. Brasselet, *Opt. Express* **18**, 14859 (2010).
  - [46] D. J. Maitland and J. T. Walsh, *Lasers in Surgery and Medicine* **20**, 310 (1997).
  - [47] I. Gusachenko, G. Latour, and M. C. Schanne-Klein, *Opt. Express* **18**, 19339 (2010).
  - [48] R. M. Korol, H. M. Finlay, M. J. Josseau, A. R. Lucas, and P. B. Canham, *J. Biomed. Opt.* **12**, 024011, 024011 (2007).
  - [49] R. W. Boyd, *Nonlinear Optics* (Academic Press, 2008), 3rd edn.
  - [50] H. W. Wang *et al.*, *Phys. Rev. Lett.* **106**, 238106 (2011).
  - [51] G. Longhi, R. Gangemi, F. Lebon, E. Castiglioni, S. Abbate, V. M. Pultz, and D. A. Lightner, *J. Phys. Chem. A* **108**, 5338 (2004).
  - [52] N. Berova, L. Di Bari, and G. Pescitelli, *Chem. Soc. Rev.* **36**, 914 (2007).
  - [53] I. Rocha-Mendoza, D. R. Yankelevich, M. Wang, K. M. Reiser, C. W. Frank, and A.

- Knoesen, *Biophys. J.* **93**, 4433 (2007).
- [54] P. K. Johansson and P. Koelsch, *J. Am. Chem. Soc.* **136**, 13598 (2014).
  - [55] J. H. C. Wang, *J. Biomech.* **39**, 1563 (2006).
  - [56] T. A. H. Jarvinen, T. L. N. Jarvinen, B. B. Kannus, L. Jozsa, and M. Jarvinen, *J. Orthop. Res.* **22**, 1303 (2004).
  - [57] M. E. Llewellyn, R. P. J. Barretto, S. L. Delp, and M. J. Schnitzer, *Nature* **454**, 784 (2008).
  - [58] A. Zoumi, A. Yeh, and B. J. Tromberg, *Proc. Natl. Acad. Sci. U. S. A.* **99**, 11014 (2002).
  - [59] B. J. Burke, A. J. Moad, M. A. Polizzi, and G. J. Simpson, *J. Am. Chem. Soc.* **125**, 9111 (2003).